

Tunable formation of copper metal, oxide, chloride and hydroxyl chloride nanoparticles from aqueous copper solutions using nanoscale zerovalent iron particles

Richard Crane¹ and Devin Sapsford²

Abstract

The influence of different parameters (solid–liquid ratio, initial pH, initial Cu concentration and anion type) on the cementation of aqueous copper (Cu) with nanoscale zerovalent iron (nZVI) has been studied. The work has been established to study both the influence such parameters have on the kinetics and efficacy of the cementation process but also the physicochemical composition of resultant Cu-bearing products. The nZVI exhibited high Cu removal capacity (maximum removal 905.2 mg/g) due to its high surface area. X-ray diffraction determined the most common Cu-bearing precipitates were Cu_2O , CuCl_2 and $\text{Cu}_2(\text{OH})_3\text{Cl}$ for solutions containing Cl^- counterions (CuCl_2 salt precursor), while Cu^0 and Cu_2O were the most common phases for those containing SO_4^{2-} counterions (CuSO_4 salt precursor). Transmission electron microscopy determined such precipitates were discrete nanoparticles of relatively high purity Cu (e.g. >80 wt% Cu or ≥ 99.9 wt% Cu and O). Overall the results demonstrate nZVI as effective for the one-pot transformation of aqueous Cu into a range of different high purity Cu-bearing nanoparticles. The methodology developed herein is therefore likely to have important application in the recovery of Cu from wastewater and process solutions where the direct upcycling to high-value Cu-bearing nanoparticles is an advantageous form in which to recover Cu.

Keywords

Nanoscience, remediation, waste valorisation, in situ leach mining, hydrometallurgy

Date received: 11 June 2019; accepted: 24 September 2019

Topic: Nanoparticles and Colloids

Topic Editor: Tao Zhu

Associate Editor: Paola Prete

Introduction

Copper (Cu) remains a valuable commodity due to its wide-spread use in a range of different industrial and domestic products and processes (electric circuitry, transportation, metallurgy, construction, medicine, petroleum refining, etc.). The concurrent global transition towards a circular economy means that there is strong current demand for the development of new processes that can be used to recover Cu during hydrometallurgical processing. Even more pressing is the need to find economically viable means in

¹ Camborne School of Mines, College of Engineering, Mathematics and Physical Sciences, University of Exeter, Penryn Campus, Penryn, Cornwall, UK

² School of Engineering, Cardiff University, Queen's Building, The Parade, Cardiff, UK

Corresponding author:

Richard Crane, University of Exeter, Exeter EX4 4PY, UK.

Email: r.crane@exeter.ac.uk



which to capture aqueous Cu when it is present as a component of wastewaters and effluents, for example, those derived from mining, processing and disposal of Cu.¹ Furthermore, whilst Cu is an essential trace element exposure to excess Cu is known to cause a wide range of health and environmental issues, with permissible limits given by the World Health Organisation (WHO) for dissolved Cu in drinking water currently 2 mg/L² and contamination of water resources with Cu a significant global environmental problem. Therefore, the development of reliable and cost-effective methods for the removal/capture of Cu from wastewaters and effluents is an important technical challenge for environmental protection and prevention of Cu 'leakage' from the materials loop.

Conventional methods for the removal of Cu ions from solution include adsorption, precipitation and ion exchange. Among them, chemical precipitation (often by lime or sulphide salts) has become one of the most widely applied due to its low cost. However, the relatively high solubility of Cu²⁺ dictates that relatively high quantities of reagents are often required, resulting in large quantities of sludge,³ with the disposal of such sludge adding an additional cost and environmental concern.³

Rather than creating secondary waste (which requires disposal), the direct formation of functional Cu-based materials and products would be much more beneficial, because it would enable dissolved Cu to be efficiently recycled with minimal unwanted by-products. Cementation is a hydrometallurgical process that involves the precipitation of a dissolved metal ion by another more electropositive metal through an electrochemical reaction. Various researchers have studied cementation reactions for different metal ions such as gold (Au), aluminium (Al) and zinc (Zn). Cu is considered to be one of the most valuable metals which can be recovered by this technique, with a number of studies documenting the efficient cementation of Cu onto Fe⁰.⁴ Indeed, before being superseded by solvent extraction methods, cementation was the principal method that Cu was recovered during hydrometallurgical processing of Cu ores. While the use of Fe⁰ for Cu cementation in mining is therefore now redundant, the process remains highly suitable for Cu removal in effluent treatment applications due to the relatively low cost of zerovalent iron (ZVI) as a reagent.

In recent years, nanoscale zerovalent iron (nZVI) has gained much attention for its use in a wide range of water treatment applications due to its unique properties, including extremely high surface area to volume ratio and an ability to be injected into the subsurface as a colloidal suspension,⁵⁻⁸ The high efficacy of nZVI for the removal of Cu²⁺ has been reported in a number of empirical studies,^{9,10}; however, very little information currently exists on the physicochemical properties of the resultant Cu particles (particle size, particle shape, crystallinity, etc.) when removed from solution by nZVI. Indeed, if the cementation

reaction of aqueous Cu with nZVI could be harnessed to produce discrete and pure Cu nanoparticles, then the value of the Cu in the aqueous waste stream could significantly increase when compared to extracting Cu simply as a bulk scale material (e.g. a plate or nugget). Cu-based nanomaterials have received much attention due to their unique catalytic, optical, electrical and antifungal/antibacterial applications. For example, Cu₂O is a p-type semiconductor with a direct bandgap of 2 eV, which makes it a highly promising material for the conversion of solar energy into electrical or chemical energy.¹¹ Moreover, monometallic and Cu oxide nanoparticles have received much attention due to their unique antimicrobial properties while also being significantly lower cost than more conventional Ag-based (nano)materials.¹² Recent research has also demonstrated that nanostructured copper cathodes (namely nanoscale Cu₂O) are among the most efficient and selective catalysts to date for the electrochemical reduction of carbon dioxide into multicarbon products.¹³ Nanoscale Cu chloride and Cu chloride hydroxide forms have also received much attention in recent years due to their unique physicochemical properties. Among these materials, paratacamite (Cu₂(OH)₃Cl) is one of the most thermodynamically stable alkaline copper chloride phases and is known to exhibit unique applications in a wide range of sectors including catalysis,¹⁴ corrosion prevention,¹⁵ agriculture¹⁶ and the uptake and storage of hydrogen.¹⁷ Moreover various forms of cupric and cuprous chloride are used as catalysts in a wide range of reactions including the Wacker process, the production of chlorine by oxychlorination and the synthesis of numerous different chlorinated organic compounds.

In this work, the cementation reaction between nZVI and aqueous Cu has been investigated under a range of different chemical conditions. Various researchers have studied the impact of different experimental parameters on the cementation reaction between aqueous Cu and bulk scale Fe⁰ (i.e. micron scale particles or larger); however, similar experiments using nZVI are currently lacking in the literature. This work has therefore been established to provide this fundamental mechanistic data but also provide specific insight into the physicochemical composition of Cu-bearing (nano)material products, including data on the extent at which the composition of such (nano)materials (metallic, oxide, hydroxide, chloride, etc.) is influenced by the chemistry of the Cu-bearing precursor solution.

Materials and methods

Synthesis of nZVI particles

Pure nZVI was synthesised following the methodology first described by Glavee et al.,¹⁸ and then adapted by Wang and Zhang¹⁹; 7.65 g of FeSO₄·7H₂O was dissolved in 50 mL of Milli-Q water (>18.2 MΩ cm), and then a 4 M NaOH

solution was used to adjust the pH to 6.8. The salts were reduced to nZVI by the addition of 3.0 g of sodium borohydride (NaBH_4). The nanoparticle product was isolated from the aqueous phase via centrifugation (Sigma 3-16L centrifuge, 4000 r/min ($3077 \times g$) for 240 s), rinsed with absolute ethanol (approximate ratio of 50 mL/g of nZVI) and then centrifuged (Sigma 3-16L centrifuge, 4000 r/min ($3077 g$) for 240 s). This step was then repeated three more times. The nanoparticles were dried in a vacuum desiccator (approximately 10^{-2} mbar) for 48 h and then stored in an argon filled (BOC, 99.998%) MBraun (MB-acryl GB 2202-P-VAC) glovebox until required.

Experimental procedure

Four 200 mL solutions were synthesised using reagent grade CuCl_2 salt (Sigma Aldrich, 222011) comprising Cu at 50, 100, 500 and 1000 mg/L. A further three 200 mL solutions were also synthesised using CuCl_2 salt with Cu at 1000 mg/L. The pH of these solutions was adjusted to pH 2.0, 3.0 and 4.0 using a few drops of 0.1 and, where appropriate, 1 M concentration HCl. The same process was then conducted but using CuSO_4 salt (Sigma Aldrich, C1297) and 1 M H_2SO_4 for pH modification. All solutions were stored in 250-mL clear soda lime glass jars (Fisher Scientific, 11704329) and left for 24 h to equilibrate before commencing each experiment. The nZVI was added to each batch system at a concentration of 0.1 g/L and immediately sonicated for 240 s using an ultrasonic bath (Grant, XB3). Each batch system was then placed on the benchtop and periodically tested for pH and Eh. The pH probe was calibrated prior to each measurement. The measured oxidation/reduction potential (ORP) values were converted to Eh values by subtracting the difference between the measured ORP of the reference solution and the theoretical ORP of the reference solution (220 mV). Nanoparticle suspensions were extracted from each batch system at the same time. Prior to sampling each jar was gently agitated to ensure homogeneity and then 10 mL was removed using an auto-pipette. The extracted suspensions were then centrifuged at 4000 r/min ($3077 \times g$) for 240 s. The supernatant was then filtered through a 0.2 μm cellulose acetate filter and acidified (HNO_3 , 2% by volume) for inductively coupled optical emission spectrometry (ICP-OES) analysis. The nanomaterial plug (at the base of the centrifuge) was then washed using absolute ethanol (approximate ratio of 5 mL/mg of nZVI) and then centrifuged at 4000 r/min ($3077 \times g$) for 240 s again. The supernatant was then decanted. The resultant solid material was then pipetted onto a glass optical microscope slide (Agar Scientific, G251P) and an Au-coated holey carbon film (TAAB, C062/G) for X-ray diffraction (XRD) and high-resolution transmission electron microscopy (HR-TEM) analysis, respectively. Samples were dried in a vacuum chamber at $<1 \times 10^{-2}$ mbar for a minimum of 2 h prior to analysis. All sorption-desorption experiments

were conducted at room temperature (measured to be $20 \pm 1^\circ\text{C}$) and ran as duplicates, with the average data used to create the figures/tables displayed herein.

Analysis techniques

X-ray photoelectron spectroscopy (XPS) spectra were collected using a Thermo Scientific K-Alpha+ XPS spectrometer. Spectra were collected at a pass energy of 40 eV for narrow scans and 150 eV for survey scans with a 0.1 and 1 eV step respectively. Charge neutralisation was achieved using a combination of low-energy electrons and argon ions. Spectra were quantified in CasaXPS using Scofield sensitivity factors and an energy dependence of -0.6 . Curve fitting was carried out using Pisce software (Dayta Systems Ltd, 2011)²⁰ with binding energy values of the recorded lines referenced to the adventitious hydrocarbon C1s peak at 284.8 eV. To determine the relative proportions of Fe^{2+} and Fe^{3+} in the sample analysis volume, curve fitting of the recorded Fe $2p_{3/2}$ photoelectron peaks was performed following the method of Scott et al.²¹ The Fe $2p_{3/2}$ profile was fitted using photoelectron peaks at 706.7, 709.1, 710.6 and 713.4 eV corresponding to Fe^0 , Fe^{2+} octahedral; Fe^{3+} octahedral and Fe^{3+} tetrahedral. These parameters were selected on the basis that the surface oxide was assumed to be a mixture of wüstite and magnetite, as the oxide Fe^{2+} is in the same coordination with the surrounding oxygen atoms in both forms of oxide. Brunauer-Emmett-Teller (BET) surface area analysis was performed using a Quantachrome NOVA 1200 surface area analyser, with N_2 as the adsorbent and following a seven-point BET method. Prior to analysis, the samples were degassed under vacuum (approximately 10^{-2} mbar) for a 24 h period at a temperature of 75°C . Samples were ran as triplicates with the average recorded. Inductively coupled plasma optical emission spectrometry (ICP-OES) analysis of aqueous samples (to determine Cu and Fe concentrations) was performed using a Perkin Elmer Optima 2100 DV ICP-OES. A Phillips Xpert Pro X-ray diffractometer with a CoK_α radiation source was used for XRD analysis (generator voltage of 40 keV and tube current of 30 mA). XRD spectra were acquired between 2 h angles of 10 – 90° , with a step size of 0.02 and a 2 s dwell time. Data were fitted with using X-pert HighScore Plus software. HR-TEM analyses were performed using a JEOL JEM-2100 microscope at 200 kV. Energy dispersive X-ray (EDX) analysis and mapping was performed using Oxford Instruments X-MaxN analyzer and Aztec software. A beryllium sample holder was used to prevent any background Cu from being detected. Nanoparticle size distribution from TEM images was measured using ImageJ software (Java 1.6.0_24) with 50 nanoparticles analysed per sample. Samples were prepared for zeta potential analysis by synthesising 20 mL CuCl_2 or CuSO_4 bearing

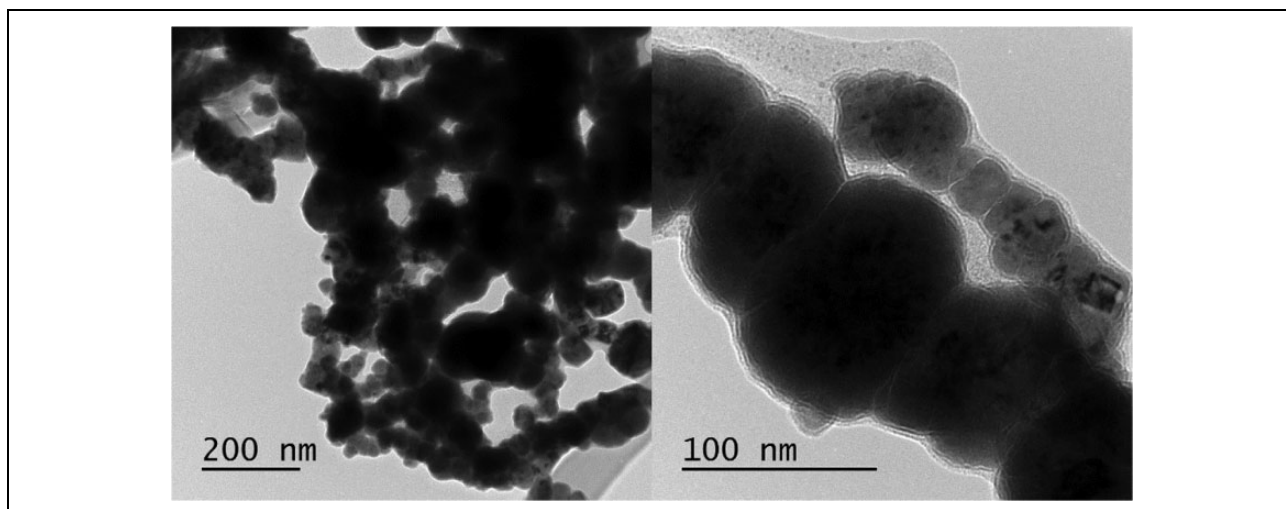


Figure 1. TEM images of the unreacted nZVI. TEM: transmission electron microscopy; nZVI: nanoscale zerovalent iron.

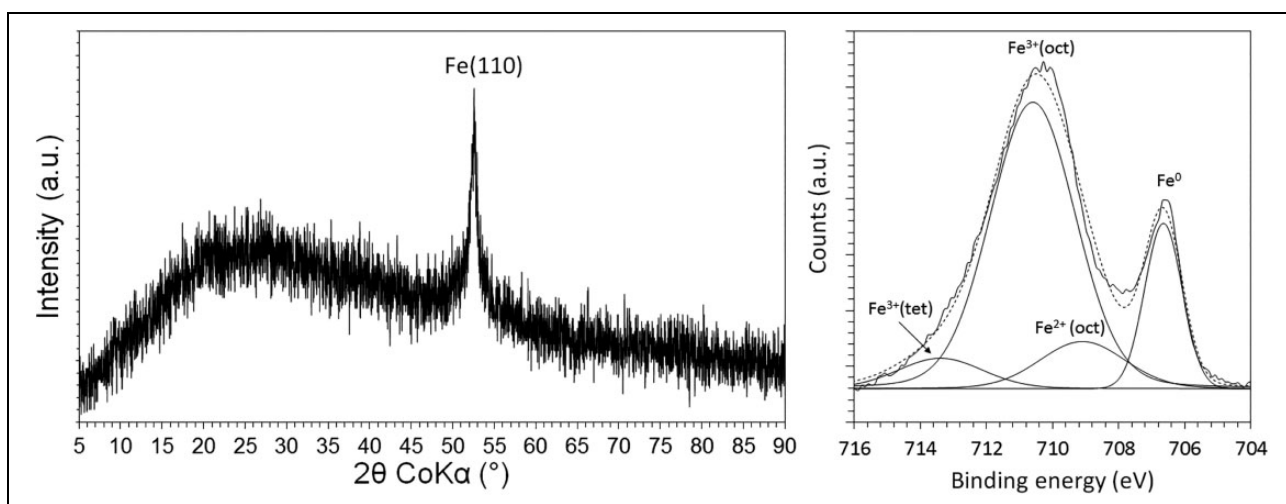


Figure 2. XRD (LHS) and curve fitted Fe $2p_{3/2}$ XPS spectra (RHS) for the unreacted nZVI. XRD: X-ray diffraction; nZVI: nanoscale zerovalent iron.

solutions with Cu at 1000 mg/L. To each batch system, nZVI was added at a concentration of 0.1 g/L. The nanoparticle suspensions were then sonicated for 240 s using an ultrasonic bath (Grant, XB3) and then left on the benchtop in the open laboratory. Each suspension was then centrifuged at 4000 r/min ($3077 \times g$) for 240 s. The supernatant was then decanted, and 40 mL of absolute ethanol was added. The suspension was then centrifuged at 4000 r/min ($3077 \times g$) for 240 s; 40 mL of a 0.1 M NaCl solution was then added. The zeta potential of the nanoparticles was then measured using a ZetaSizer Nano ZS instrument (Malvern Instruments Ltd). A refractive index of 1.86 and 0.46 was used for the nanoparticles formed from CuCl_2 and CuSO_4 solutions, respectively (corresponding to CuCl and Cu respectively) and an absorbance of 0.1. The pH was adjusted prior to each measurement using HCl or NaOH at 0.1 M concentrations.

Results and discussion

Characterisation of the unreacted nZVI

TEM analysis determined that the nZVI were spherical, generally within an approximate size range of 10–150 nm and an average diameter of 61 nm (Figure 1). Each individual nZVI particle was recorded to contain a discrete outermost layer (density contrast), which is attributed to be the presence of an oxide shell surrounding the Fe^0 core. In addition, dark mottles were recorded within the metallic cores which indicate that individual particles are either polycrystalline or comprised of isolated metal crystals in an otherwise amorphous matrix. Individual nZVI particles were recorded as aggregated into chains and rings due to their high surface energy and magnetic properties.²² BET surface area analysis determined that the surface area of the nZVI was $50.9 \text{ m}^2/\text{g}$. A single diffraction peak at $52.381^\circ 2\theta$ was recorded using XRD and attributed to be the (110)

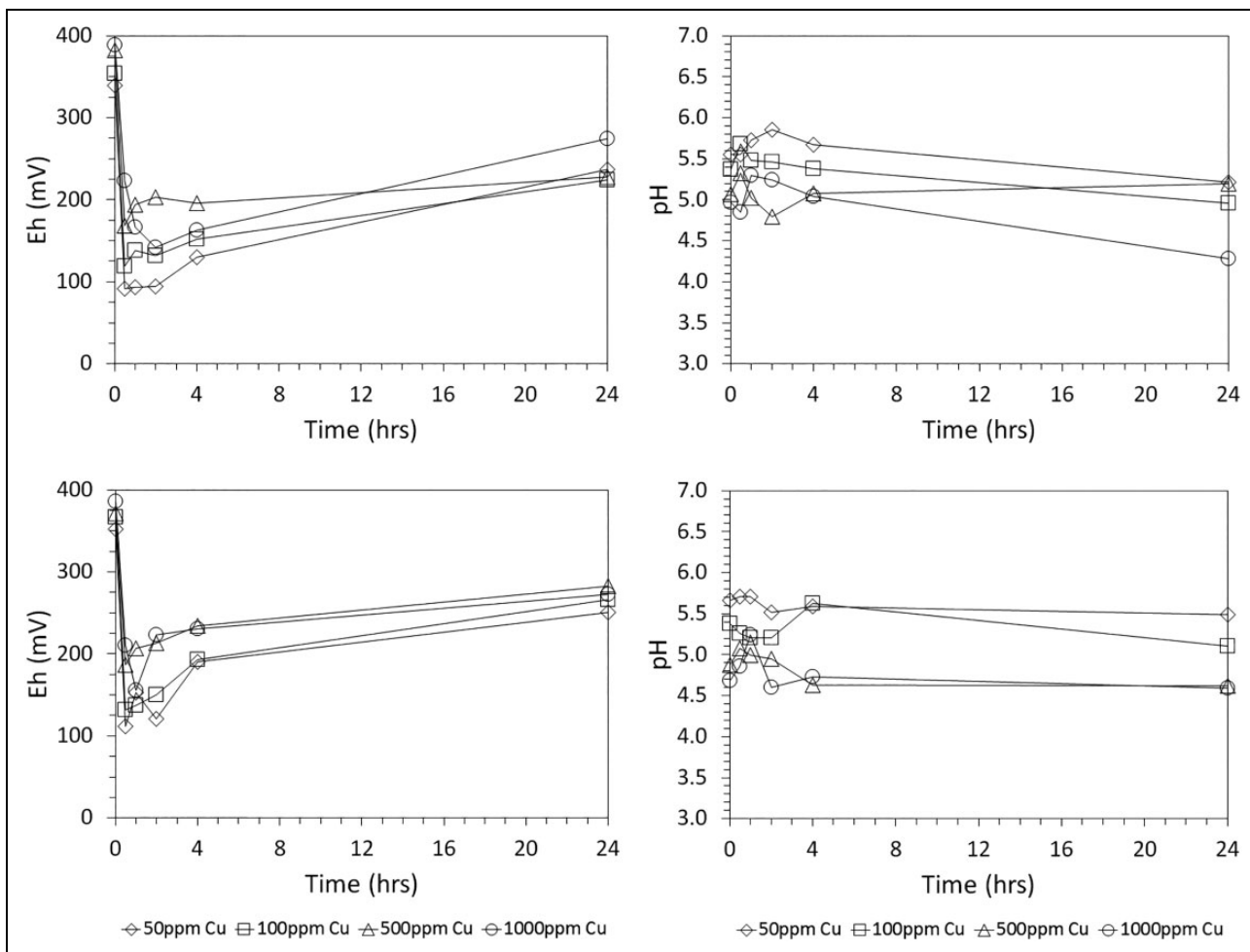


Figure 3. Eh and pH as a function of time for batch systems containing 50, 100, 500 and 1000 mg/L Cu for batch systems containing CuCl_2 (top) and CuSO_4 (bottom). An nZVI concentration of 0.1 g/L was used. nZVI: nanoscale zerovalent iron; Cu: copper.

lattice reflection of $\alpha\text{-Fe}^0$ (Figure 2). The peak is recorded as relatively broad which indicates that the nZVI are somewhat amorphous. XPS analysis recorded the outer surface of the nZVI to be comprised of a mixed valent ($\text{Fe}^{2+}/\text{Fe}^{3+}$) oxide (Figure 3) overlying a Fe^0 core. Given the mean free path of Fe is equivalent to approximately five atomic layers, this detection of Fe^0 in the XPS analysis volume therefore indicates that the oxide thickness is less than approximately 5 nm, which corresponds well with the aforementioned nZVI oxide thickness measurement using TEM. Results are summarised in Table 1 and concur with previous characterisation studies of nZVI,^{23–26}

Changes in pH and Eh

For all experimental systems, the addition of nZVI to the solutions resulted in a rapid decrease in Eh and a concurrent increase in pH (Figures 3 and 4). Eh minima were recorded

Table 1. Bulk and surface properties of the nZVI.^a

Parameter	Analysis technique	nZVI
Particle size distribution (%)	TEM	0–50 nm: 32.1 50–100 nm: 58.5 >100 nm: 9.4
Bulk composition	XRD	$\alpha\text{-Fe}^0$
Oxide thickness (nm)	XPS	3–5
Specific surface area (m^2/g)	BET	50.9
Surface composition (at%)	XPS	B: 16.0 C: 5.3 O: 52.7 Na: 8.1 Fe: 17.9
Fe stoichiometry ($\text{Fe}^{2+}/\text{Fe}^{3+}$)	XPS	0.15
Fe stoichiometry ($\text{Fe}^0/\text{Fe}^{2+} + \text{Fe}^{3+}$)	XPS	0.19

^a A significant proportion of the carbon detected is likely to be adventitious carbon.

TEM: transmission electron microscopy; nZVI: nanoscale zerovalent iron.

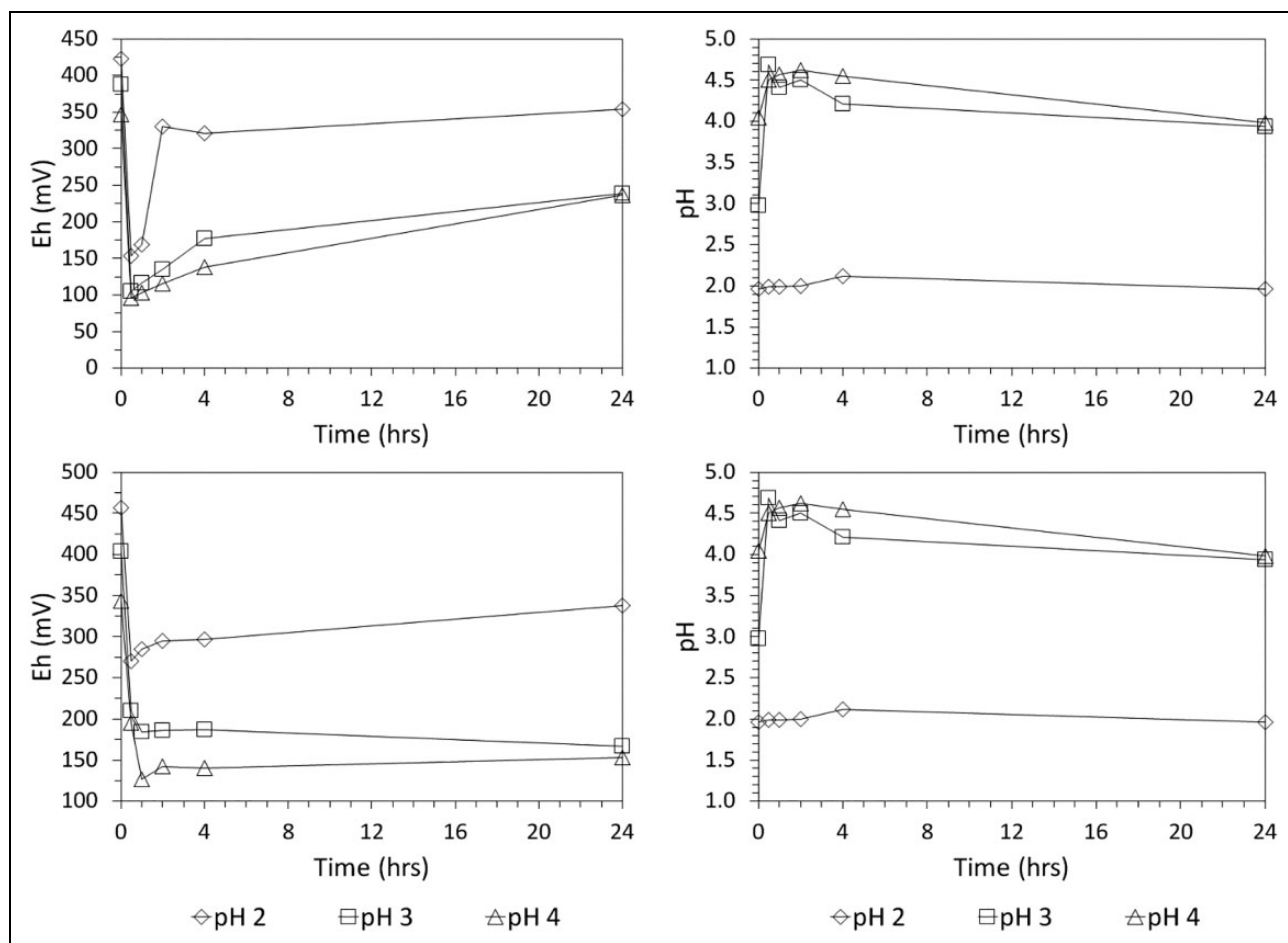


Figure 4. Eh and pH as a function of time for batch systems containing 1000 mg/L Cu for batch systems containing CuCl_2 (top row) or CuSO_4 (bottom row) at a starting pH of 2.0, 3.0, and 4.0. An nZVI concentration of 0.1 g/L was used. nZVI: nanoscale zerovalent iron; Cu: copper.

within the first 2 h of reaction for all systems, while pH maxima were all recorded within the first 4 h of reaction. This behaviour is attributed to the rapid oxidation of the nZVI surfaces during their initial exposure to the Cu-bearing solutions, consuming dissolved oxygen (DO) and H^+ and increasing the reduction potential of the system. Following this initial nZVI reaction period (e.g. <4 h), a recovery in pH and Eh was recorded in all systems, with reversal to near ambient (pre nZVI addition) conditions recorded for all systems recorded after 24 h.

No clear difference in changes in Eh and pH was recorded for batch systems with different starting Cu concentrations (Figure 3). In contrast, a marked difference was recorded for batch systems with different starting pH, with the greatest change typically recorded for the batch systems with the highest starting pH (Figure 4). For example, Eh minima were recorded as 245, 197 and 188 mV for the batch systems containing Cl^- and with starting pH of 2, 3 and 4, respectively. Similarly, Eh minima were recorded as 362, 259 and 219 for the

batch systems containing SO_4^{2-} and with starting pH of 2, 3 and 4, respectively. This is attributed to the acidic dissolution of the nZVI at lower pH which in turn decreases the quantity of the nanomaterial available to scavenge oxygen and decreases the reduction potential of the solution.

Changes in the concentrations of Cu and Fe ions

In all systems, most significant Cu removal (and simultaneous Fe dissolution) was recorded during the initial stages of the reaction (typically <4 h; Figures 5 to 7). In general, the greatest removal of Cu from solution was recorded for systems containing the highest starting Cu concentrations, and greater Cu uptake was general recorded for solutions containing SO_4^{2-} than those containing Cl^- . For example, maximum removal of 513.2, 816.2, 977.7 and 818.0 mg of Cu per gram of original nZVI was recorded for CuSO_4 solutions with Cu at a starting concentration of 50, 100, 500 and 1000 mg/L, respectively, and an nZVI concentration of 0.1 g/L compared to 369.7, 472.8, 387.8 and 848.5

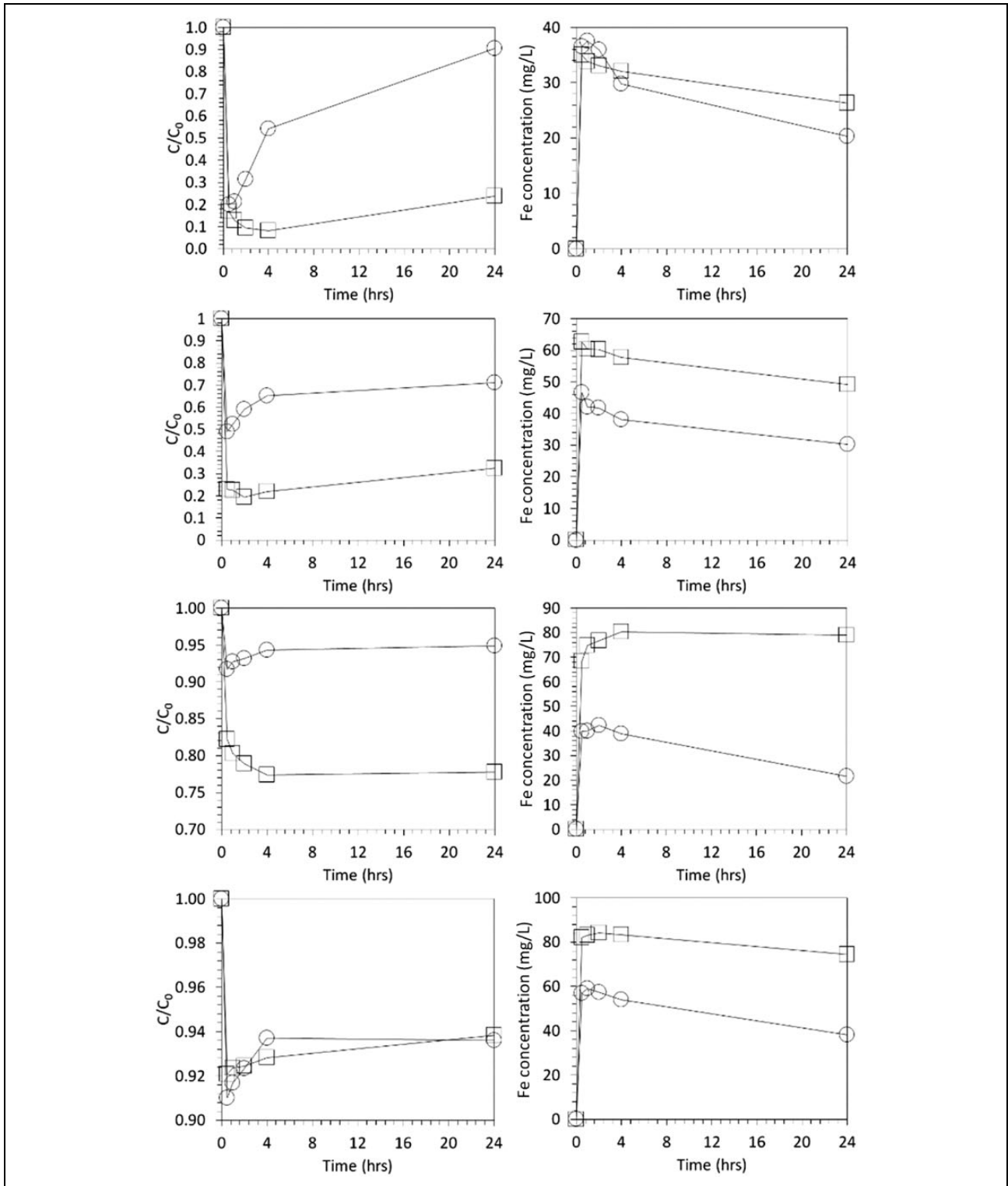


Figure 5. Normalised Cu concentrations (C/C_0) and absolute Fe concentrations (mg/L) as a function of time in each batch system (circle markers: solutions containing CuCl_2 , square markers: solutions containing CuSO_4). From top to bottom: 50, 100, 500 and 1000 mg/L starting Cu concentration. An nZVI concentration of 0.1 g/L was used. Starting pH was 4.5–6 (see Figure 3). nZVI: nanoscale zerovalent iron; Cu: copper.

for CuCl_2 solutions with Cu at a starting concentration of 50, 100, 500 and 1000 mg/L, respectively. Similarly, maximum uptake of 578.0 and 895.6 mg of Cu per gram of

original nZVI was recorded for CuCl_2 and CuSO_4 solutions respectively, each with Cu at a starting concentration of 1000 mg/L and nZVI at a concentration of 1.0 g/L (Figure

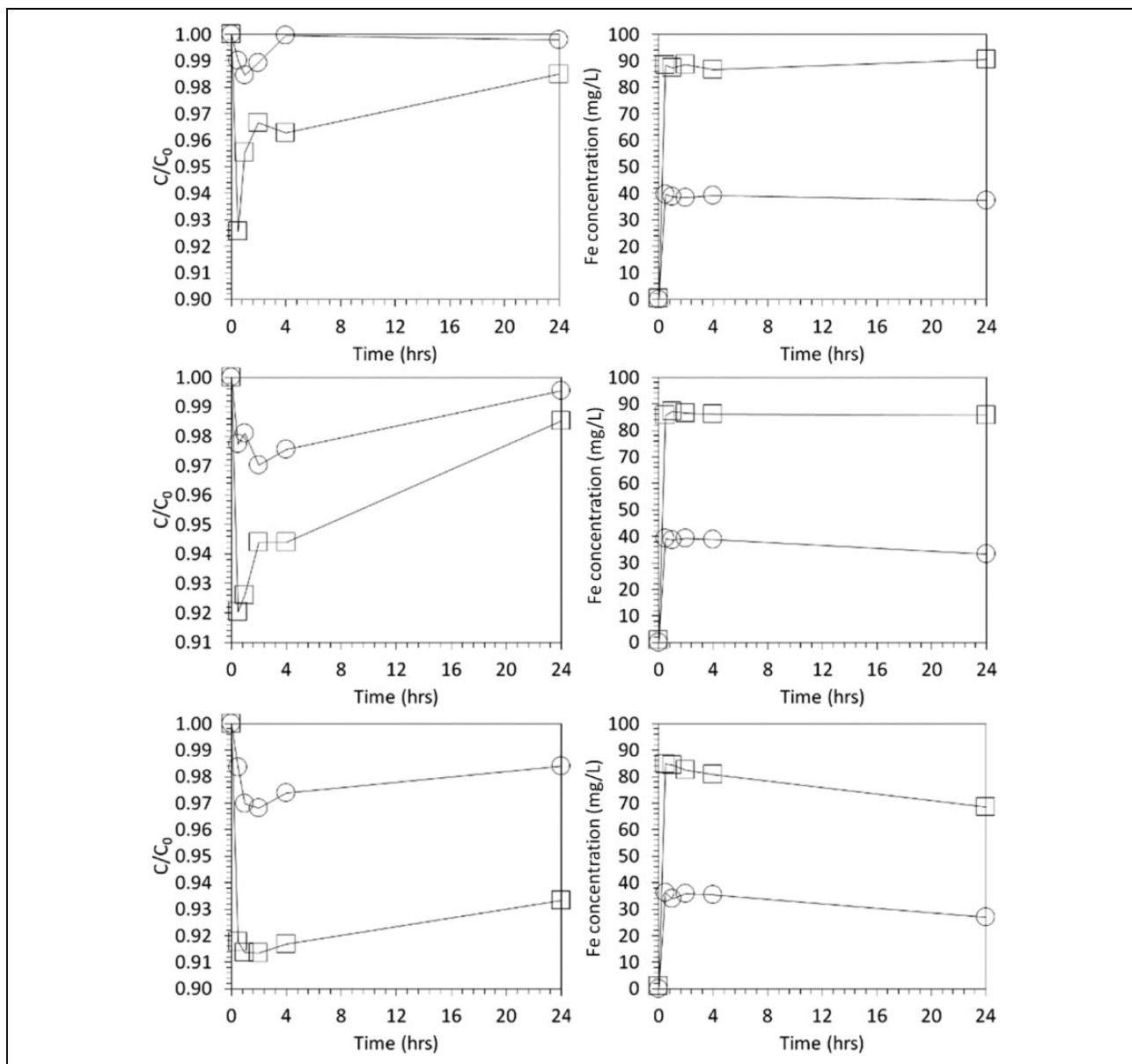
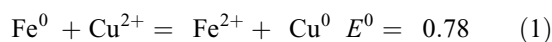


Figure 6. Normalised Cu concentrations (C/C_0) and absolute Fe concentrations (mg/L) as a function of time in each batch system containing 1000 mg/L Cu (circle markers: the CuCl_2 systems, square markers: the CuSO_4 system). Top row: starting pH = 2.0; middle row: starting pH = 3.0; bottom row: starting pH = 4.0. An nZVI concentration of 0.1 g/L was used. nZVI: nanoscale zerovalent iron; Cu: copper.

7). Results therefore also demonstrate that a greater nZVI starting concentration directly results in greater total Cu removal, due to the greater mass of the nanomaterial for Cu ion cementation (which is also reflected in the greater dissolved Fe recorded) and enhanced DO consumption which subsequently results in stronger chemically reducing conditions being established.

Starting pH exhibited a clear influence on Cu uptake, with greater total Cu removal generally recorded at higher pH. For example, maximum uptake of 784.1, 833.1 and 905.2 mg/g was recorded for CuSO_4 solutions with a starting pH of 2.0, 3.0 and 4.0 respectively

compared to 155.0, 298.9 and 321.1 for CuCl_2 solutions, respectively. The standard reduction potential (E^0) of Cu/Cu^{2+} and Fe/Fe^{2+} couples is 0.34 and -0.44 V, respectively, and as such the removal of Cu onto nZVI is ascribed to the simultaneous oxidation (and dissolution) of Fe^0 and chemical reduction of Cu^{2+} via the following cementation reaction:



Following this initial Cu uptake period, a slight increase (typically <10%) in aqueous Cu concentrations was recorded for all systems. This suggests that a proportion

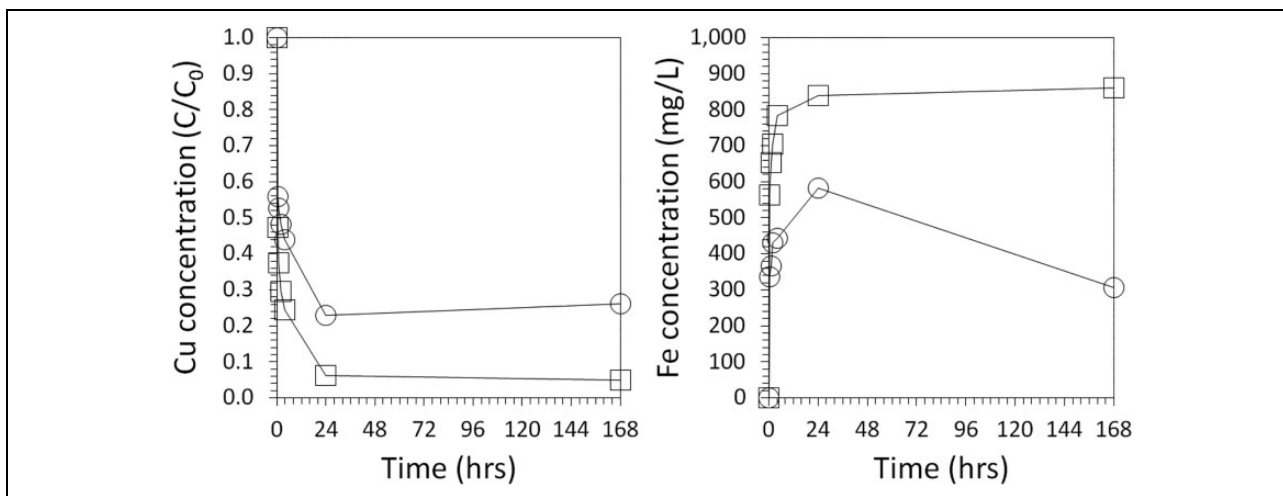


Figure 7. Normalised Cu concentrations (C/C_0) and absolute Fe concentrations (mg/L) as a function of time in each batch system containing 1000 mg/L Cu (circle markers: the CuCl_2 systems, square markers: the CuSO_4 system). An nZVI concentration of 1 g/L and an initial pH of 4.0 was used for each system. nZVI: nanoscale zerovalent iron; Cu: copper.

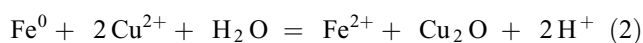
of the solid Cu that was removed from solution via cementation with nZVI was in a relatively reactive state and as such dissolved back into solution in the latter stages of the experiment concurrent with a reversal in both solution pH and Eh to ambient (pre nZVI addition) conditions. No clear correlation between the extent of Fe dissolution and the starting concentrations of CuCl_2 or CuSO_4 was recorded; however, a correlation was recorded with the starting pH of the solution, with greatest Fe dissolution typically recorded at low pH. After 24 h exposure of the Cu-bearing solutions to nZVI at a 0.1 g/L concentration, aqueous Fe concentrations were recorded to be 20.3, 30.3, 21.5 and 38.2 mg/L for batch systems containing Cl^- as the counterion (50, 100, 500 and 1000 mg/L aqueous Cu starting concentrations respectively) and 26.3, 49.2, 79.0 and 74.5 mg/L for batch systems containing SO_4^{2-} as the counterion (50, 100, 500 and 1000 mg/L aqueous Cu starting concentrations respectively). This correlates to 79.7%, 69.7%, 78.5%, and 61.8% of Fe remaining in the solid phase (as original nZVI or as corrosion products and/or precipitates) for the Cl^- containing solutions, compared to 73.7%, 50.8%, 21.0% and 25.5% for the SO_4^{2-} -bearing solutions. This result therefore demonstrates that SO_4^{2-} resulted in greater total nZVI corrosion than Cl^- , which is attributed to the higher anion charge density exhibited by the former anion, as previously noted for bulk scale Fe^0 (e.g. cm scale Fe^0 coupons²⁷).

XRD data

The XRD data demonstrate that Cu^0 and Cu_2O phases are the most common products for solutions containing CuSO_4 , while Cu_2O , CuCl_2 and $\text{Cu}_2\text{Cl}(\text{OH})_3$ predominate for solutions containing CuCl_2 (Figures 8 and 9). The only batch system to record a Fe-bearing XRD pattern was the system containing SO_4^{2-} as the anionic species and a starting Cu

concentration of 50 mg/L, where a minor contribution from lepidocrocite ($\gamma\text{-FeOOH}$) was recorded. This demonstrates that minimal quantities of crystalline nZVI corrosion products were present in all systems, that is, the majority of precipitated Fe is likely to have been amorphous. XRD spectra for the batch system containing CuCl_2 at 50 mg/L recorded Cu_2O as the only crystalline phase present, while a mixture of Cu_2O , CuCl_2 and $\text{Cu}_2\text{Cl}(\text{OH})_3$ was recorded for the batch system containing CuCl_2 at ≥ 100 mg/L. This demonstrates that there is a threshold of approximately 100 mg/L CuCl_2 required to form crystalline CuCl_2 bearing phases (i.e. to above the detection limit of our XRD system). In addition, batch systems containing starting concentrations of CuCl_2 at 1000 mg/L and a starting pH of 3 and 4 resulted in a mixture of CuCl_2 and $\text{Cu}_2\text{Cl}(\text{OH})_3$, indicating that such phases can readily form at low pH (Figure 9). The presence of different concentrations of $\text{CuSO}_4(\text{aq})$ resulted in no clear difference in the composition of nanomaterial products, with a mixture of Cu^0 and Cu_2O recorded for all batch systems irrespective of starting CuSO_4 concentration or pH. Cu^0 was detected throughout the entire 24-h reaction period for all systems containing SO_4^{2-} as the counterion, which indicates that it is relatively stable nanomaterial.

Overall the results demonstrate that in systems containing relatively low concentrations of Cl^- (e.g. <100 mg/L), Cu_2O is the dominant Cu-bearing product, with its formation likely via equation (2). In contrast, in systems containing SO_4^{2-} as the counterion, both Cu^0 and Cu_2O are recorded to form equations (1) and (2). This suggests that either Cl^- interferes with cementation reaction or Cu^0 was formed initially but was subsequently oxidised to Cu_2O



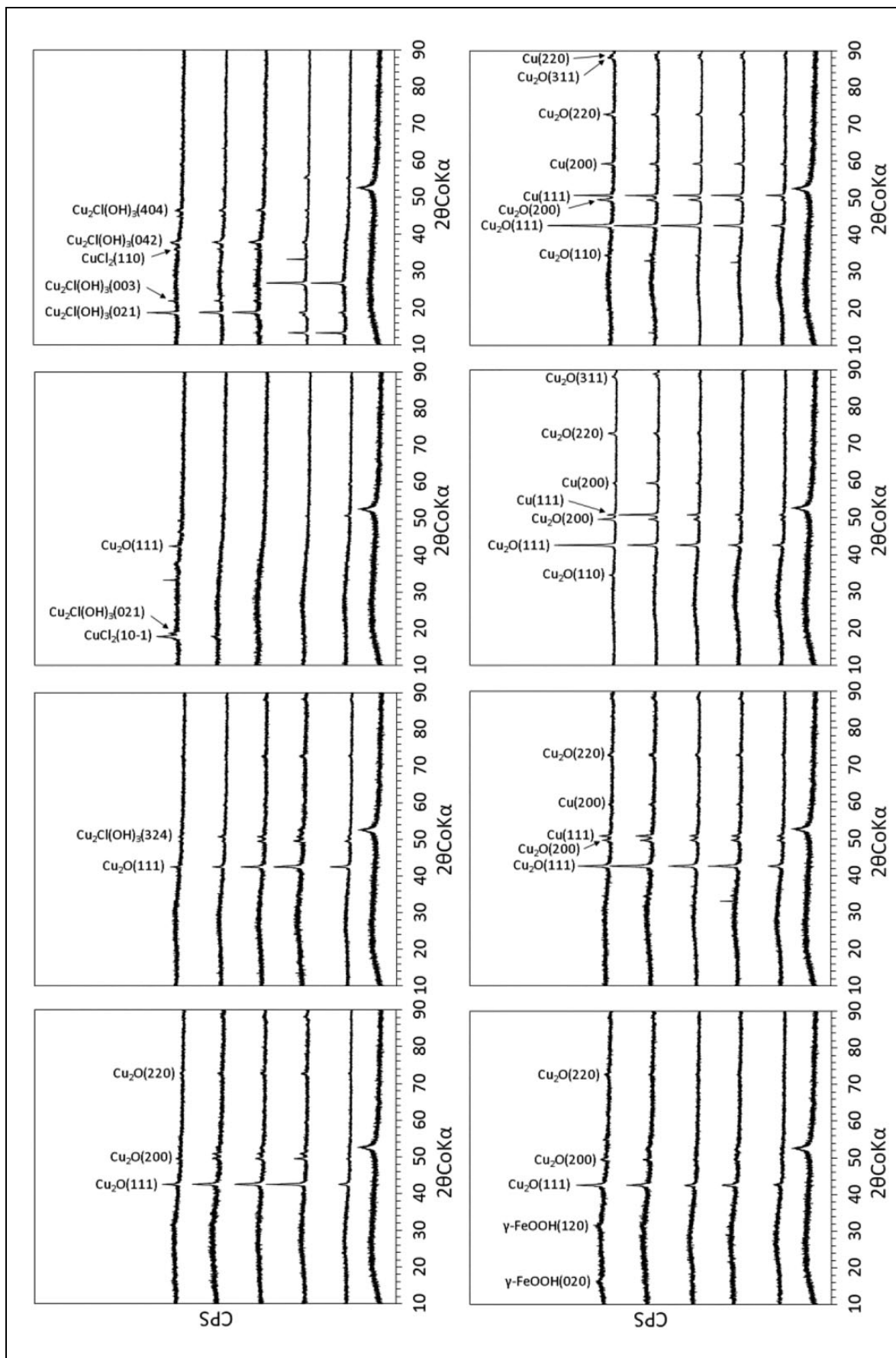


Figure 8. XRD spectra recorded for nZVI extracted from solutions containing CuCl_2 (top row) or CuSO_4 (bottom row) at 50, 100, 500 and 1000 mg/L (from left to right). Spectra are for the nZVI extracted from each system after 0, 0.5, 1, 2, 4 and 24 h reaction time (stacked from bottom to top). An nZVI concentration of 0.1 g/L was used. Starting pH was 4.5–6 (see Figure 3). XRD: X-ray diffraction; nZVI: nanoscale zerovalent iron; Cu: copper.

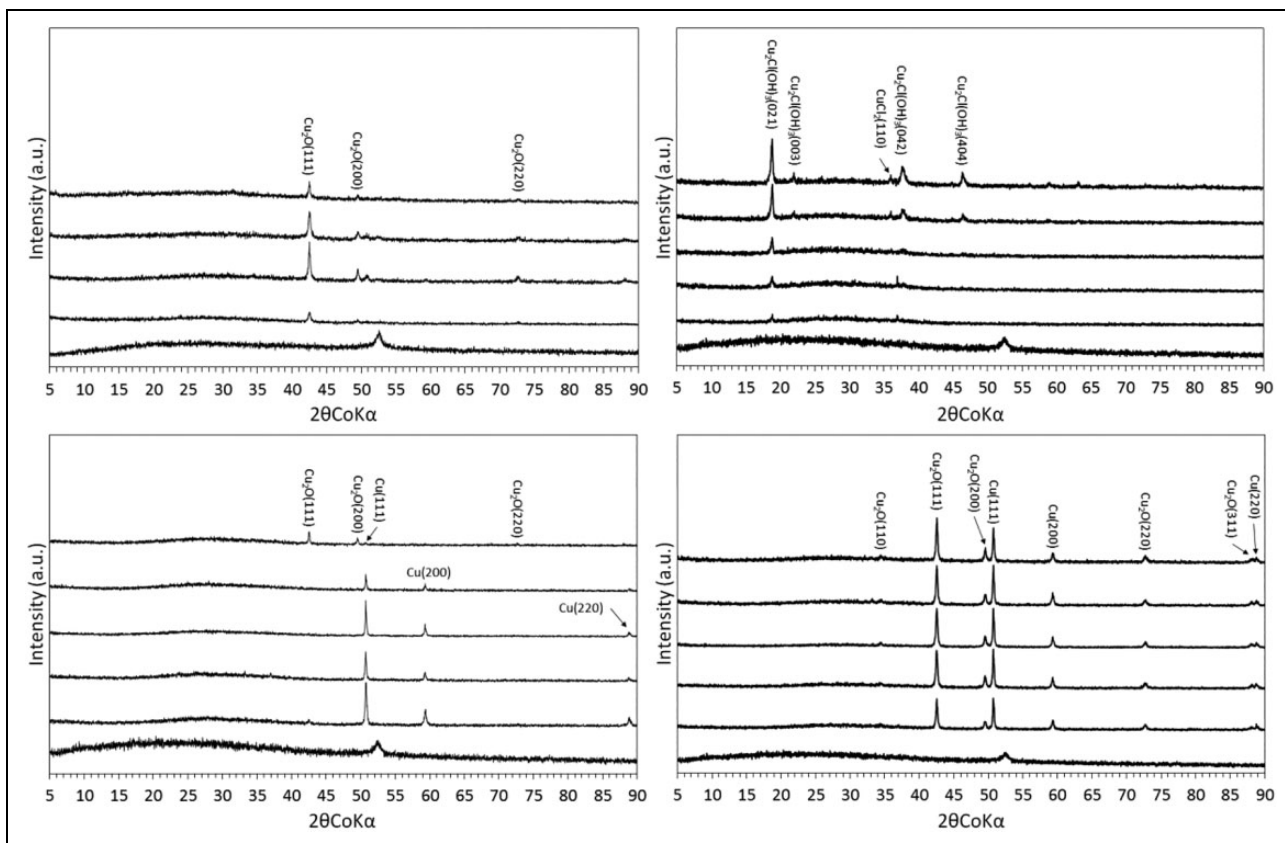


Figure 9. XRD spectra recorded for nZVI extracted from solutions containing CuCl_2 (top row) or CuSO_4 (bottom row) at a starting pH of 3.0 (LHS) and 4.0 (RHS). Spectra are for the nZVI extracted from each system after 0, 0.5, 1, 2, 4 and 24 h reaction time (stacked from bottom to top). It was not possible to record XRD spectra for the systems with a starting pH of 2.0 due to acidic dissolution resulting in insufficient material being present. XRD: X-ray diffraction; nZVI: nanoscale zerovalent iron.

Using equation (2) Cu^{2+} is reduced to cuprite at an Fe to Cu molar ratio of 1:2, and this may explain (in part) the relatively high reduction capacity (e.g. >500 mg Cu per g nZVI) recorded herein.

TEM data

TEM images of the nZVI after 4 h reaction with the 1000 mg/L CuCl_2 or CuSO_4 solutions, along with EDX data of the four most common elements (by wt%) present, are displayed in Figures 10 and 11. Two distinct types of nanomaterial can be observed in both figures, hereafter referred to as ‘needles’ and ‘spherical’ nanoparticles, with the former comprised predominantly of Fe and O, and the latter comprised predominantly of Cu and O. Corroborating these data with the XRD data, it can therefore be stated that the needle-shaped nanoparticle are likely to be nZVI corrosion products (i.e. largely composed of amorphous iron (hydr)oxides), whereas the spherical particles are likely to be a mixture of Cu^0 and Cu_2O nanoparticles, which have formed via cementation ((1) and (2)). This result is significant because it proves that the Cu and Fe nanomaterials formed in this current work are separate discrete nanomaterials and as such will be able to be

separated from each other (e.g. selective dissolution). Physical and chemical properties of the Cu-bearing nanoparticles formed due to the exposure of 1000 mg/L solutions of CuCl_2 and CuSO_4 to 0.1 g/L nZVI for 4 h. It can be noted that both types of nanomaterial are polycrystalline with a relatively high sphericity. The nanoparticles formed from CuCl_2 salts were typically of lower purity than those derived from CuSO_4 salts, with the maximum Cu purity detected of 48.4 and 83.3 wt% Cu, respectively. The nanoparticles derived from CuSO_4 salts were also recorded to be smaller than those derived from CuCl_2 and also more rounded in shape.

Zeta potential data

Figure 12 displays zeta potential (ζ) measurements as a function of solution pH for the Cu-bearing nanoparticles which have formed from the exposure of the nZVI to CuCl_2 or CuSO_4 solutions at 1000 mg/L for 24 h. It can be seen that a different ζ range was recorded for the nZVI which have been exposed to CuCl_2 or CuSO_4 solutions, with maximum of 8.5 and 16.2 mV recorded for each nanoparticle type at a pH of 3.3 and 3.2, respectively, and a minimum of -14.0 and -16.2 mV recorded for each nanoparticle type

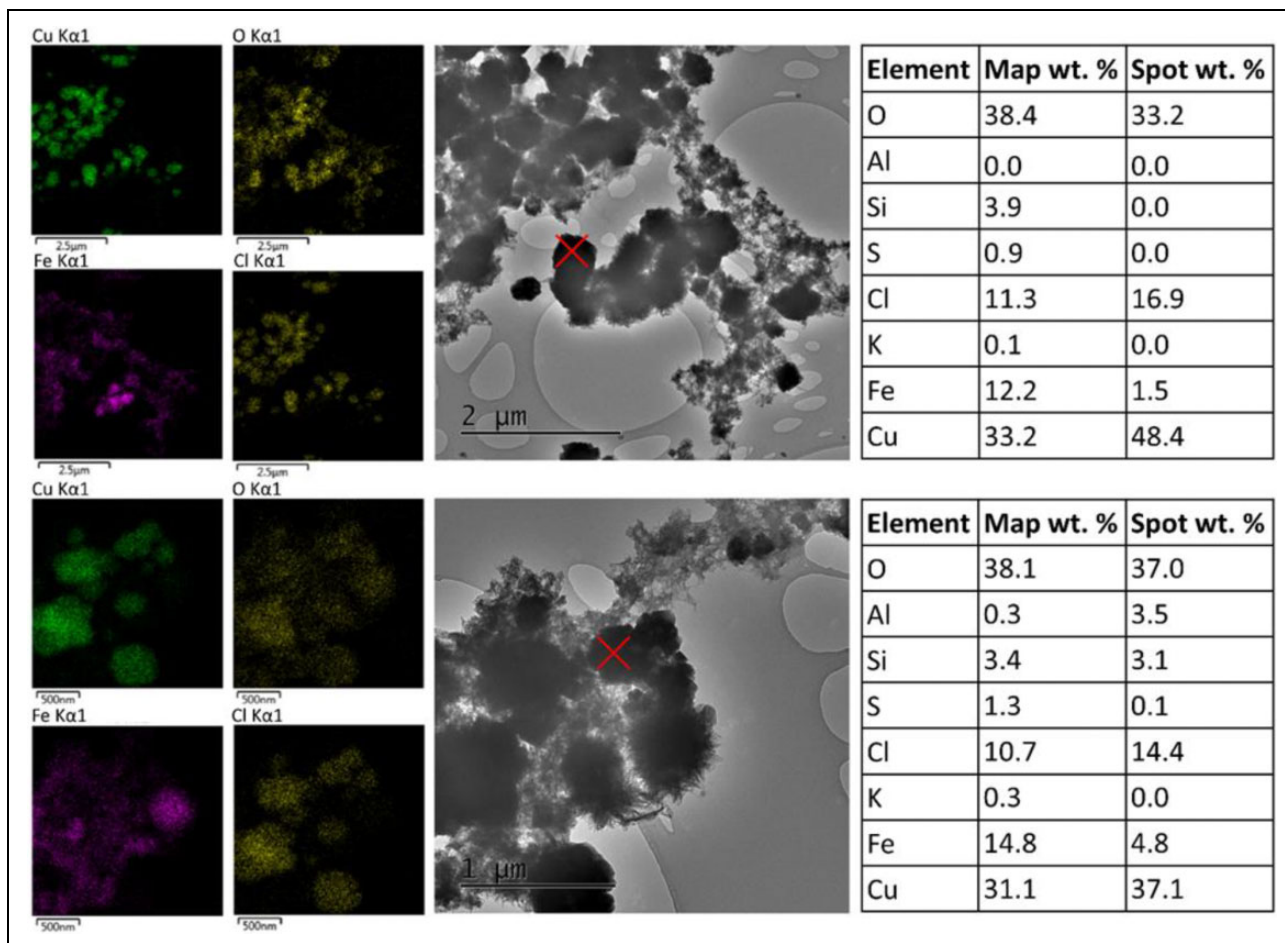


Figure 10. TEM images of the nZVI after 4 h reaction with a 1000 mg/L CuCl_2 solution, along with EDX maps of the four most common elements (by wt%) present. Composition (wt%) recorded using EDX for the overall map and spot (marked in red) is also displayed. An nZVI concentration of 0.1 g/L was used. TEM: transmission electron microscopy; EDX: energy dispersive X-ray; nZVI: nanoscale zerovalent iron.

at a pH of 12.1 and 11.9, respectively. The point of zero charge (PZC) is recorded as much lower for the nZVI which have been exposed to CuCl_2 solution compared to the nZVI which have been exposed to the CuSO_4 solutions, with a PZC recorded to be at a pH of approximately 6.7 and 10.5, respectively. The differences in ζ versus pH (along with the XRD data displayed in Figure 8) further confirm that the products formed in the CuSO_4 and CuCl_2 systems are physicochemically distinct. It is often assumed that colloids with a ζ of >40 mV possess high stability in the aqueous phase.²⁸ It can therefore be stated that both nanomaterial types are likely to exhibit relatively limited long-term stability in the aqueous phase.

Industrial/environmental implications

Electrowinning and electrorefining are the most common conventional routes for the recovery of Cu from both aqueous sources (waste water, lixivants, etc.) and impure metals (e.g. blister Cu), respectively, with the objective

of both methods the formation of a high-purity, often highly crystalline, Cu electroplate deposit at the cathode. The resultant Cu sheets are then extracted and sold directly as a raw material which are then subsequently transformed into Cu-bearing products for uses in a wide range of applications. The synthesis of Cu nanoparticles from such sheets is then typically conducted via: (i) dissolution of the sheet into an electrolyte which is followed by a nanoparticle recovery method (e.g. chemical precipitation or chemical reduction) or (ii) mechanical, thermal or sonochemical decomposition (e.g. ball milling, ultrasound). A key economic limit associated with this process, therefore, is that these processes require several expensive and energy intensive steps. Instead if Cu nanoparticles could be synthesised *directly* from the aqueous Cu source (e.g. Cu-bearing mining leachate, Cu-bearing waste water), then the process would be fundamentally more efficient. Here we have demonstrated that nZVI could be used as a highly effective reagent to selectively produce high-purity Cu nanoparticles (83.3% Cu, $>99.9\%$ Cu and O) directly from aqueous Cu

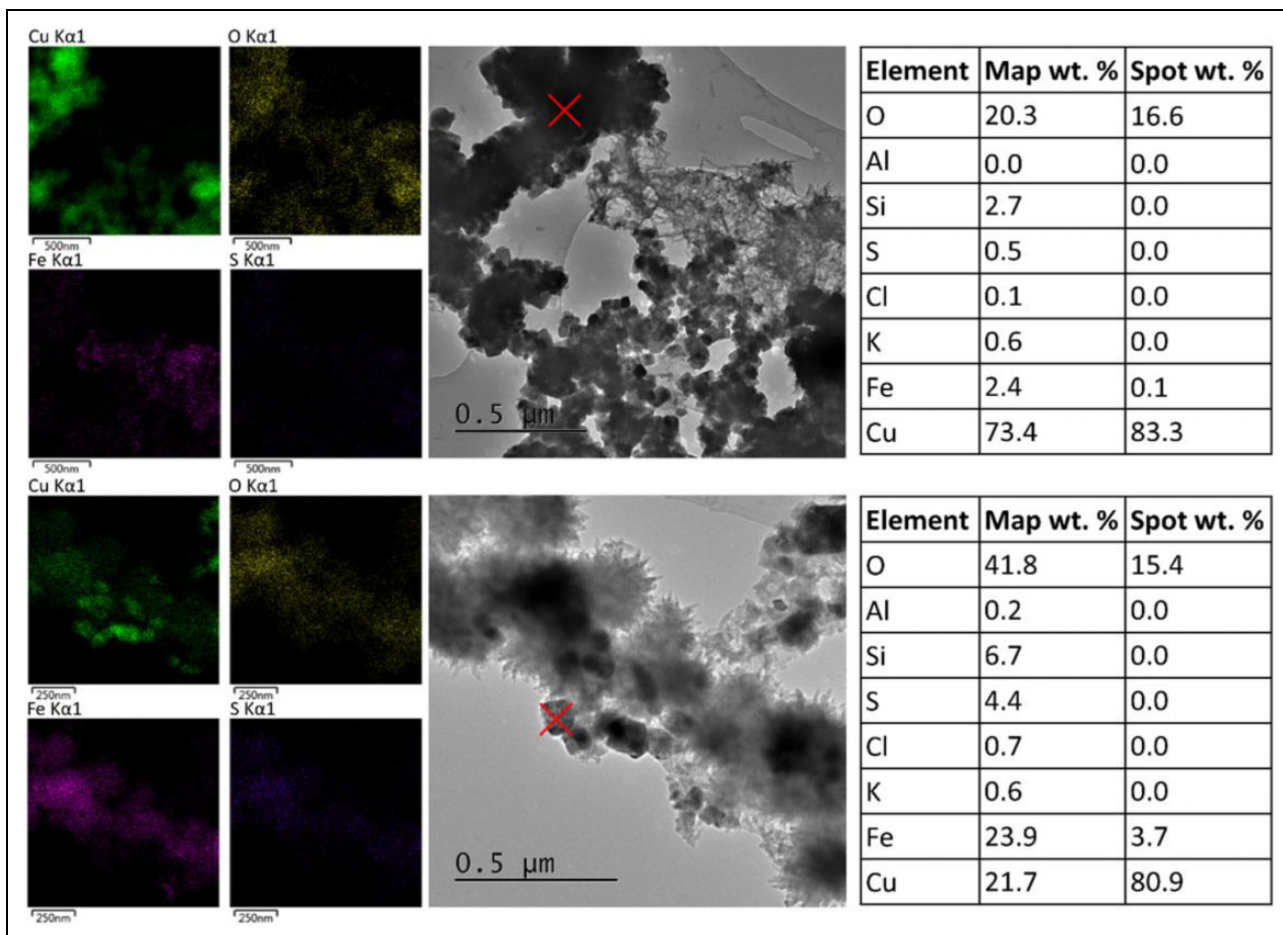


Figure 11. TEM images of the nZVI after 4 h reaction with a 1000 mg/L CuSO_4 solution, along with EDX maps of the four most common elements (by wt%) present. Composition (wt%) recorded using EDX for the overall map and spot (marked in red) is also displayed. An nZVI concentration of 0.1 g/L was used. TEM: transmission electron microscopy; EDX: energy dispersive X-ray; nZVI: nanoscale zerovalent iron.

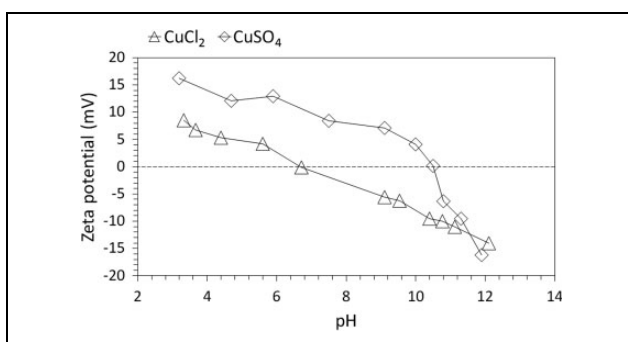


Figure 12. Zeta potential (mV) as a function of pH for the nanoparticles formed following the exposure of nZVI (concentration of 0.1 g/L) to 1000 mg/L CuCl_2 and CuSO_4 solutions for 24 h. nZVI: nanoscale zerovalent iron.

sources via a one-pot process that does not require any electrical input. The use of nZVI is also particularly useful because it is selective for Cu nanoparticle formation from mixed aqueous systems.^{29,30} The results demonstrate that the process is highly adaptable and can result in the

formation of high purity Cu-bearing nanoparticles of various different physical structures and chemistry. For example, Table 2 displays an overview of the different physical and chemical properties of Cu-bearing nanoparticles formed via the exposure of aqueous Cu (as 1000 mg/L solutions of CuCl_2 and CuSO_4) with 0.1 g/L nZVI for 4 h. In contrast, the use of a more powerful chemical reducing agent (such as NaBH_4) would exhibit less selectivity than nZVI and thus chemically reduce a mixture of present metals (e.g. Cu, Fe, Co, Ag) resulting in a nanomaterial of mixed chemical composition that likely has limited functionality. This work therefore provides a key first step in the emerging research field into the development of next generation methodologies for the selective and direct formation of engineered nanomaterials from aqueous sources. In particular, this research could be particularly applicable for the selective recovery of Cu from aqueous waste streams (e.g. acid mine drainage, industrial effluents), where the significantly greater economic gain generated by the direct formation of high-value engineered nanomaterials (rather than Cu plates from electrowinning) could be used to

Table 2. Physical and chemical properties of the Cu-bearing nanoparticles formed due to the exposure of 1000 mg/L solutions of CuCl₂ and CuSO₄ to 0.1 g/L nZVI for 4 h.

Parameter	Analysis technique	Cu nanoparticles (derived from CuCl ₂ salts)	Cu nanoparticles (derived from CuSO ₄ salts)
Particle size distribution (%)	TEM	0–50 nm: 9.1 50–100 nm: 13.6 >100 nm: 77.3	0–50 nm: 52.2 50–100 nm: 43.5 >100 nm: 4.3
Mean particle size (nm)	TEM	201.1	51.7
Bulk composition	XRD	Cu ₂ O, Cu ₂ Cl(OH) ₃	Cu ⁰ , Cu ₂ O
Maximum purity detected (wt% Cu)	TEM-EDX	48.4	83.3
Nanoparticle shape	TEM	High sphericity, angular	High sphericity, subrounded
Crystallinity	TEM	Polycrystalline	Polycrystalline
Point of zero charge (pH)	Zeta potential	6.7	10.5

XRD: X-ray diffraction; TEM: transmission electron microscopy; EDX: energy dispersive X-ray; nZVI: nanoscale zerovalent iron.

significantly offset the cost of such waste water treatment processes.

Conclusions

Waste valorisation is a critical research field because it acts to both safeguard the environment but also protect essential material supply chains. A relatively unexplored yet extremely promising strand of this research is the development of methodologies for the direct formation of functional nanomaterials from waste because it has the potential to impart dramatic cost savings due to the substantially high economic value of certain nanomaterials when compared to their bulk scale counterpart.

Here the influence of different chemical factors (namely, solid–liquid ratio, starting pH, starting Cu concentration and anion type) on the cementation of aqueous Cu with nZVI has been studied. The work has been established to investigate the mechanisms and kinetics of Cu removal from solution but in particular the physicochemical composition of resultant Cu-bearing cemented (nano)particles. The following can be concluded:

- (1) The nZVI exhibited exceptionally high Cu removal capacity (maximum removal recorded was 905.2 mg/g) due to the high purity and reactivity of the nZVI.
- (2) Starting pH exhibited a relatively strong influence on the extent of Cu uptake with greatest Cu removal from solution and retention in the solid phase recorded for batch systems at a starting pH of 4.0.
- (3) Type of anion(s) present in the Cu-bearing solution exhibited a clear influence on both the extent of Cu removal but also the type of Cu nanoparticulate products formed, with Cu₂O, CuCl₂ and Cu₂(OH)₃Cl determined as the most common nanoparticulates formed for the batch systems containing Cl[−] as the counterion, while Cu⁰ and Cu₂O

were the most common phases formed in systems containing SO₄^{2−} as the counterion.

- (4) Starting pH exhibited no discernible influence on the bulk chemical composition (phase) of Cu nanoparticles formed via cementation of CuSO₄ solutions with nZVI, with a mixture of Cu⁰ and Cu₂O recorded for all system studies. In contrast, starting pH exhibited a clear influence on the bulk chemical composition of Cu nanoparticles formed via cementation of CuCl₂ solutions with nZVI, with Cu₂O recorded as the main phase present for Cu formed from CuCl₂ solutions with a starting pH of 3.0, compared to a mixture of Cu₂Cl(OH)₃ and CuCl₂ recorded for solutions with a starting pH of 4.0.
- (5) TEM analysis determined the Cu-bearing nanoparticles to be extremely high purity (e.g. >80 wt% Cu or ≥99.9 wt% Cu and O) which were recorded as among, but not chemically bound to, needle-shaped nZVI amorphous corrosion products.
- (6) Solid liquid separation of Cu-bearing nanoparticles must occur relatively quickly after nZVI addition (e.g. within 4 h) to prevent Cu re-release (redissolution).

Overall the results demonstrate nZVI as a highly effective scavenger of aqueous Cu, with the one-pot formation of discrete high-purity Cu-bearing nanoparticles which could then be directly used in a wide range of applications. Future work will investigate how nZVI selectivity for metal high-purity nanoparticle formation can be fine-tuned for operation in increasingly complex environments (e.g. mixed contaminant systems and/or water bodies containing complex combinations of background solutes). In addition, the sourcing of nZVI from cheaper materials (e.g. waste streams) would also be highly beneficial to improve the economic return of such processes.

Acknowledgements

We would like to thank Mr Jeff Rowlands and Mr Marco Santonastaso and from the School of Engineering, Cardiff University

for their technical support. We would also like to thank Dr Thomas Davies from the Cardiff Catalysis Institute and the Cardiff Electron Microscopy Facility for the TEM analysis. Photographs included in the RHS of the graphical abstract are from the following references (clockwise from top LHS):^{31–35}


Declaration of conflicting interests

The author(s) declared no potential conflicts of interest with respect to the research, authorship, and/or publication of this article.

Funding

The author(s) disclosed receipt of the following financial support for the research, authorship, and/or publication of this article: This work was financially supported by the Natural Environment Research Council (grant no. NE/L013908/1) and the Camborne School of Mines Trust.

ORCID iD

Richard Crane  <https://orcid.org/0000-0003-0117-2245>

References

1. Crane RA, Sinnott DE, Cleall PJ, et al. Physicochemical composition of wastes and co-located environmental designations at legacy mine sites in the south west of England and Wales: implications for their resource potential. *Resour Conserv Recy* 2017; 123: 117–134.
2. WHO. *Guidelines for Drinking-Water Quality*. 4th ed. 2011. ISBN: 978 92 4 154815 1. URL. Available at: http://www.who.int/water_sanitation_health/publications/2011/dwq_guidelines/en/ (accessed 12 January 2018)
3. Kang CD, Sim SJ, Cho YS, et al. Process development for the removal of copper from wastewater using ferric/limestone treatment. *Korean J Chem Eng* 2003; 3: 482–486.
4. Shokes TE and Möller G. Removal of dissolved heavy metals from acid rock drainage using iron metal. *Environ Sci Technol* 1999; 33: 282–287.
5. Crane RA and Scott TB. Nanoscale zero-valent iron: future prospects for an emerging water treatment technology. *J Hazard Mater* 2012; 211: 112–125.
6. Crane RA, Dickinson M, Popescu IC, et al. Magnetite and zero-valent iron nanoparticles for the remediation of uranium contaminated environmental water. *Water Res* 2011; 45: 2931–2942.
7. Popescu IC, Filip P, Humelnicu D, et al. Removal of uranium (VI) from aqueous systems by nanoscale zero-valent iron particles suspended in carboxy-methyl cellulose. *J Nucl Mater* 2013; 443(1–3): 250–255.
8. Crane RA, Pullin H, Macfarlane J, et al. Field application of iron and iron–nickel nanoparticles for the ex situ remediation of a uranium-bearing mine water effluent. *J Environ Eng* 2015; 141(8): 04015011.
9. Scott TB, Popescu IC, Crane RA, et al. Nano-scale metallic iron for the treatment of solutions containing multiple inorganic contaminants. *J Hazard Mater* 2011; 186: 280–287.
10. Karabelli D, Uzum C, Shahwan T, et al. Batch removal of aqueous Cu^{2+} ions using nanoparticles of zero-valent iron: a study of the capacity and mechanism of uptake. *Ind Eng Chem Res* 2008; 47: 4758–4764.
11. Wang WZ, Wang GH, Wang XS, et al. Synthesis and characterization of Cu_2O nanowires by a novel reduction route. *Adv Mater* 2002; 14: 67–69.
12. Rai RV and Bai JA. Nanoparticles and their potential application as antimicrobials, science against microbial pathogens: communicating current research and technological advances. In: Méndez-Vilas A (ed.) *Formatex, microbiology series*, No. 3, Vol. 1, Spain, 2011, pp. 197–209.
13. Eilert A, Roberts FS, Friebel D, et al. Formation of copper catalysts for CO_2 reduction with high ethylene/methane product ratio investigated with in situ x-ray absorption spectroscopy. *J Phys Chem Lett* 2016; 7(8):1466–1470.
14. Lee JS and Park ED. In situ XAFS characterization of supported homogeneous catalysts. *Top Catal* 2002; 18(1–2): 67–72.
15. Nairn JD, Skennerton SG and Atrens A. Comparative atmospheric corrosion of primary and cold rolled copper in Australia. *J Mater Sci* 2003; 38(5): 995–1005.
16. Snyman RG, Reinecke AJ and Reinecke SA. Field application of a lysosomal assay as biomarker of copper oxychloride exposure, in the Snail *Helix Aspersa*. *Bull Environ Contam Toxicol* 2002; 69(1): 117–122.
17. Lee SC, Park SH, Lee SM, et al. Synthesis and H_2 uptake of $\text{Cu}_2(\text{OH})_3\text{Cl}$, $\text{Cu}(\text{OH})_2$ and CuO nanocrystal aggregate. *Catal Today* 2007; 120(3–4): 358–362.
18. Glavee GN, Klabunde KJ, Sorensen CM, et al. Chemistry of borohydride reduction of iron(II) and iron(III) ions in aqueous and nonaqueous media, formation of nanoscale Fe, FeB and Fe_2B powders. *Inorg Chem* 1995; 34: 28–35.
19. Wang CB and Zhang WX. Synthesizing nanoscale iron particles for rapid and complete dechlorination of TCE and PCBs. *Envir Sci Technol* 1997; 31(7): 2154–2156.
20. Dayta Systems Ltd, <http://www.daytasystems.co.uk/> (2011, accessed April 2017).
21. Scott TB, Allen GC, Heard PJ, et al. Reduction of U(VI) to U(IV) on the surface of magnetite. *Geochim Cosmochim Acta* 2005; 69(24): 5639–5646.
22. Baalousha M. Aggregation and disaggregation of iron oxide nanoparticles: influence of particle concentration, pH and natural organic matter. *Sci Tot Environ* 2009; 407: 2093–2101.
23. Scott TB, Dickinson M, Crane RA, et al. The effects of vacuum annealing on the structure and surface chemistry of iron nanoparticles. *J Nanopart Res* 2010; 12(5): 1765–1775.
24. Crane RA and Scott TB. The removal of uranium onto nanoscale zero-valent iron particles in anoxic batch systems. *J Nanomater* 2014; 2014: 1–12.
25. Crane RA, Pullin H and Scott TB. The influence of calcium, sodium and bicarbonate on the uptake of uranium onto nanoscale zero-valent iron particles. *Chem Eng J* 2005; 277: 252–259.
26. Crane RA and Scott TB. The effect of vacuum annealing of magnetite and zero-valent Iron nanoparticles on the removal of aqueous uranium. *J Nanotechnol* 2013; 2013: 1–11.

27. Peng CY, Ferguson JF and Korshin GV. Effects of chloride, sulfate and natural organic matter (NOM) on the accumulation and release of trace-level inorganic contaminants from corroding iron. *Water Res* 2013; 47: 5257–5269.
28. Yu W and Xie H. A review on nanofluids: preparation, stability mechanisms and applications. *J Nanomater* 2012; 2012: 1–17.
29. Crane RA and Sapsford DJ. Selective formation of copper nanoparticles from acid mine drainage using nanoscale zerovalent iron particles. *J Hazard Mater* 2018; 347: 252–265.
30. Crane RA and Sapsford DJ. Towards “precision mining” of wastewater: selective recovery of Cu from acid mine drainage onto diatomite supported nanoscale zerovalent iron particles. *Chemosphere* 2018; 202: 339–348.
31. <https://circuitboard.com/> (accessed 24 April 2019)
32. <https://what-is-nanotechnology.com/2Cu-CuO-Cu2O-copper-oxide-nanodots.htm> (accessed 24 April 2019)
33. <https://www.constructioncanada.net/coppers-antimicrobial-properties/> (accessed 24 April 2019)
34. <https://scanmarket.com/snapshots-repository/lubricant-oil/> (accessed 24 April 2019)
35. <http://www.kurzweilai.net/advances-in-nanotechnology-enable-targeted-drug-delivery> (accessed 24 April 2019)